Corrected 11 November 2014; see below

www.sciencemag.org/cgi/content/full/science.1259437/DC1

Supplementary Materials for

The structure of interfacial water on gold electrodes studied by x-ray absorption spectroscopy

Juan-Jesus Velasco-Velez, Cheng Hao Wu, Tod A. Pascal, Liwen F. Wan, Jinghua Guo, David Prendergast, Miquel Salmeron*

*Corresponding author. E-mail: mbsalmeron@lbl.gov

Published 23 October 2014 on *Science* Express
DOI: 10.1126/science.1259437

This PDF file includes:

Correction: The reference list has been updated.

1. Computational Methods

Classical molecular dynamics simulations

We constructed a simulation cell by placing 150 water molecules 4Å above a model of the (111) surface gold comprising 6 atomic layers. The initial cell dimensions were 11.7Å × 10.2Å × 75.0Å. After initial conjugate gradient energy minimization to an RMS force of 10^{-5} kcal/mol/Å, we performed 10ns of constant temperature (298K), constant pressure (1bar) NPT molecular dynamics (MD) simulation using the LAMMPS (*36*) simulation engine. The water molecules were described with the flexible simple point charge (SPC/Fw) water model (*37*), the gold atoms with the Embedded Atom Model of Zhou and cowokers (*38*), while the water-gold van der Waals interactions were described by the pair-potentials of Kremer and coworkers (*39*). The temperature damping constant was 0.1 ps and the simulation timestep was 1.0 fs. Long-range Coulombic interactions were calculated using the particle-particle particle-mesh (PPPM) method (*40*) (with a precision of 10^{-5} kcal/mol), while the van der Waals interactions were computed with a cubic spline (inner cutoff of 5Å and an outer cutoff of 6Å). We used the spline to guarantee that the energies and forces go smoothly to zero at the outer cutoff, thereby preventing discontinuities in the energies and forces. The equations of motion used were those of Shinoda et al. (*41*), which combine the hydrostatic equations of Martyna et al. (*42*) with the strain energy proposed by Parrinello and Rahman (*43*). We applied a barostat in the z dimension only in order to equilibrate the water density above and below the gold surface. The time integration schemes closely follow the time-reversible measure-preserving Verlet integrators derived by Tuckerman et al (*44*). The final cell dimension was 11.7Å × 10.2Å × 74.2Å.

We also performed MD simulations of a system comprising 76 water molecules and a monolayer of 35 pentane molecules. The pentane molecules were described using the General Amber Force Field (GAFF) (*45*). During dynamics, the center of mass of each pentane molecule was constrained, so that the water molecules experienced a near constant, planar hydrophobic environment.

Ab-initio molecular dynamics (AIMD) simulations for structural analysis

The equilibrated structure from our classical MD simulation was used as input for at least 100ps constant volume, constant temperature (canonical or NVT) density functional theory (DFT) MD simulation at 298K using a modified version of the mixed Gaussian and plane wave code (*46*) CP2K/Quickstep (*47*). We employed a triple-ζ basis set with two additional sets of polarization functions (TZV2P) (*48*) and a 320 Ry plane-wave cutoff. We use the Perdew-Burke-Ernzerhof (PBE) form of the generalized-gradient approximation to the unknown exchange-correlation potential in DFT (*49*) (consistent with our XAS simulations), and the Brillouin zone is sampled at the Γ-point only. Interactions between the valence electrons and the ionic cores are described by norm-conserving pseudopotentials (*50,51*). The Poisson problem is tackled using an efficient Wavelet-based solver (*52*). We overcome the poor description of the short-range dispersive forces within the PBE-GGA exchange-correlation functional by employing the DFTD3 empirical corrections of Grimme et al (*53*). Snapshots of the system were saved every step. As a figure of merit, we performed simulations on smaller cells (5.8Å x 5.1Å x 30Å – with 6 water layers, and 5.8Å x 5.1Å x 20Å – 4 water layers) and found that

convergence to the bulk density away from the interfacial region required at least 6 water layers.

Structural analysis

We analyzed the last 80ps of our CP2K AIMD trajectory (160,000 frames) and calculated the density of the water molecules next to the gold surface by discretizing the z-coordinate of the center of mass of each water atom in 0.1Å bins. The resulting mass density profile is shown in figure 2b. The position of the 1st main peak from our AIMD simulation is 3.13 Å, if the point of reference is the center of the closest surface Au atoms, or 2.63 Å from the Au surface (assuming a 0.7Å ionic radius for Au). This compares well to the results of Cicero et al (*54*) who reported a peak at 3.2Å using the center of Au surface atoms, Fernandez *et al.* (*55*) who reported a distance of 3 – 3.5Å from the center of the Au surface atoms, and Nadler and Sanz (*29*) who reported a peak position of 2.5 – 2.6 Å from the Au surface.

From the mass density profile, we partitioned water molecule into one of three shells based on their instantaneous z-coordinate: first shell molecules within 0 – 6Å of the gold surface, second shell from next 6 – 9.2 Å, and bulk molecules beyond 9.2Å.

For each water molecule we calculated the number of hydrogen bonds it participated in. Here, a hydrogen bond was present if the O – O distance was within 3.5Å and the O-O-H angle was within 35^{o} (*56*). We labeled each molecule as: double donor (DD) if both of its hydrogen atoms participated in a bond; single donor (SD) if only one hydrogen atom binds to a neighboring water molecule (i.e., with one broken hydrogen bond); and no donor (ND) with two broken hydrogen bonds. We further separated the SD species based on their relative orientation to the Au-surface: SD$^{\parallel}$ species are characterized by both OH – surface normal angles being ± 30^{o}.

AIMD simulations to obtain snapshots for XAS calculations.

Due to computational limitations related to using plane-wave calculations to simulate X-ray absorption spectra, we halved the number of water molecules and reduced the number of gold layers (from 6 to 3) with respect to our original *ab initio* simulation cells. As noted before, larger simulation cells and longer simulation times are required to obtain convergence to the bulk density at the center of the cell. However, we found that the local structure of the interfacial layer water molecules (as measured by the number of donor/acceptor hydrogen bonds) in the smaller VASP simulations (0.15 ± 0.05, 0.29 ± 0.04 and 0.53 ± 0.04 for SD$^{\parallel}$, SD$^{\perp}$ and DD species respectively) were relatively consistent with our larger/longer CP2K simulations (0.18 ± 0.05, 0.31 ± 0.04 and 0.49 ± 0.04 respectively). Thus we pre-equilibrated the smaller system as described previously and performed 10ps NVT AIMD simulations using a plane-wave basis-set truncated at 350 eV to represent the electronic wavefunctions within the projector-augmented wave (PAW) formulation (*57, 58*), as realized in the Vienna Ab Initio Simulation Package (VASP) (*59, 60*). The exchange-correlation energy is approximated using the optB86b-vdW functional to include the effect of van der Waals dispersion forces (*52*). We employed a 2x2x1 k-point grid to ensure convergence of the electron density in the supercell. Snapshots of the system were saved every step. Upon equilibration, 5 well-separated (i.e., uncorrelated) snapshots were taken from the last 5ps of the AIMD

trajectory (1 ps apart) and used in subsequent XAS calculations to establish an ensemble-averaged spectrum.

We simulated the effect of finite bias by adjusting the total number of electrons in our system, effectively raising/lowering the Fermi level of the gold. Two additional simulations were performed with an increase/decrease of 2 electrons per supercell. We note that the calculated XAS of the negative and positive bias systems were obtained by projecting the water donor populations unto the corresponding average spectra of each species from the neutral system.

XAS calculations

Oxygen K-edge spectra were calculated by exciting each oxygen atom in each snapshot individually using constrained-occupancy DFT calculations employing the PBE GGA functional (*49*). Plane–wave pseudopotential calculations using ultrasoft pseudopotentials (*61*) were performed using the PWSCF code within the Quantum-ESPRESSO package (*62*). We used a kinetic energy cut-off for electronic wave functions of 25 Ry and a density cut-off of 200 Ry The core-excited Kohn–Sham eigenspectrum was generated using the XCH approach (*23*). Based on a numerically converged self-consistent charge density, we generated the unoccupied states for our XAS calculations non-self-consistently, sufficiently sampling the first Brillouin zone with a 2×2×2 uniform k-point grid, employing an efficient implementation of the Shirley interpolation scheme (*63*) generalized to handle ultrasoft pseudopotentials (*64*). Matrix elements were evaluated within the PAW frozen-core approximation (*65*). Core-excited ultrasoft pseudopotentials and corresponding atomic orbitals were generated with the Vanderbilt code (*61*). Each computed transition was convoluted with a 0.2 eV Gaussian function to produce continuous spectra.

2. Potential calibration

During collection of the TEY XAS spectra under applied bias between the working Au electrode and the counter electrode (Pt wire) the reference electrode was disconnected to avoid fluctuations of the large Faradaic current due to the feedback from the potentiostat. The potentials shown in Fig. 4 were measured with the pseudo-reference Ag electrode in the same cell when spectra were not being collected. The point of zero charge in our system was estimated to be around 80 mV relative to the Ag quasi-reference electrode by measuring the capacitance minimum as a function of bias (figure S6).

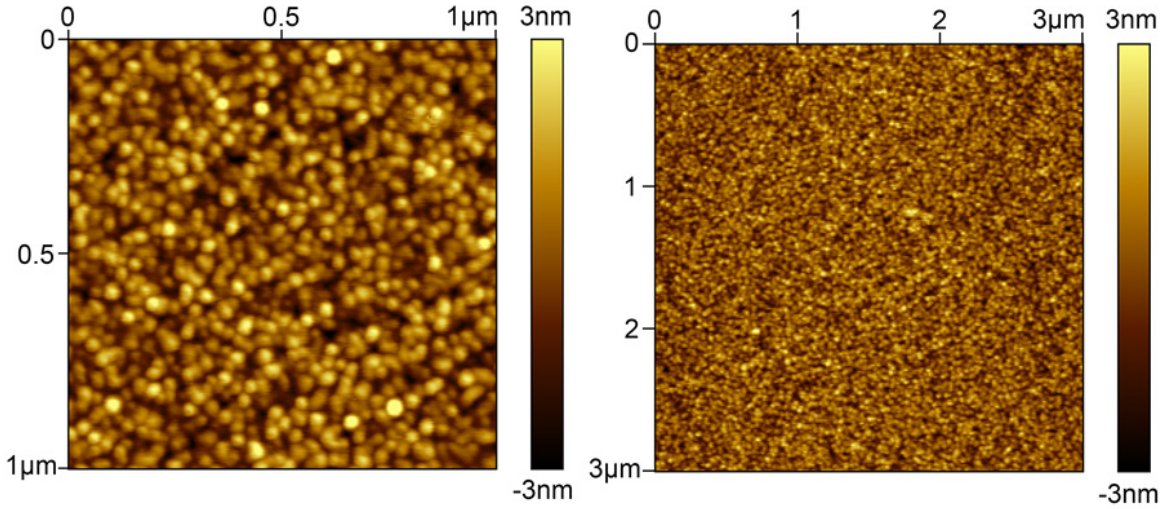

Figure S1

AFM topographical images of the surface of a 20nm Au thin film deposited on the Si_3N_4 window by thermal evaporation. The RMS values for two images are 1.00 nm and 0.76 nm, respectively.

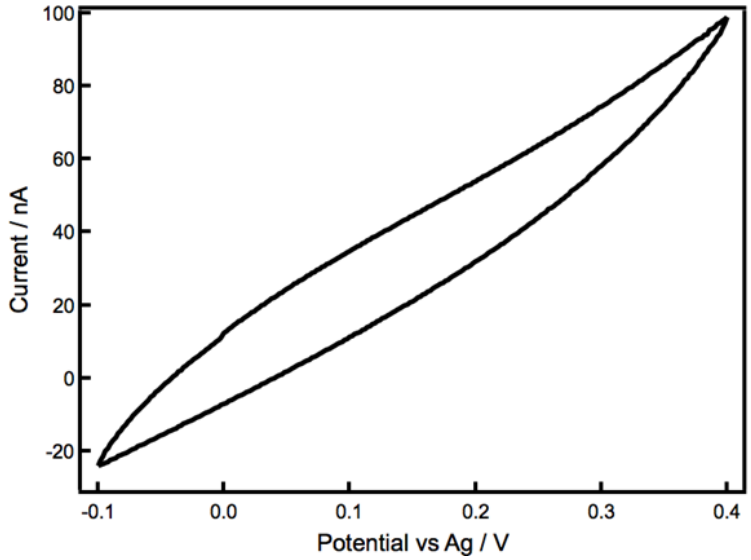

Figure S2

Cyclic voltammetry from gold-platinum electrode system in a 10µM NaCl solution measured with respect to a Ag reference electrode in the flow liquid cell used in the experiments. The scan rate is 10mV/s.

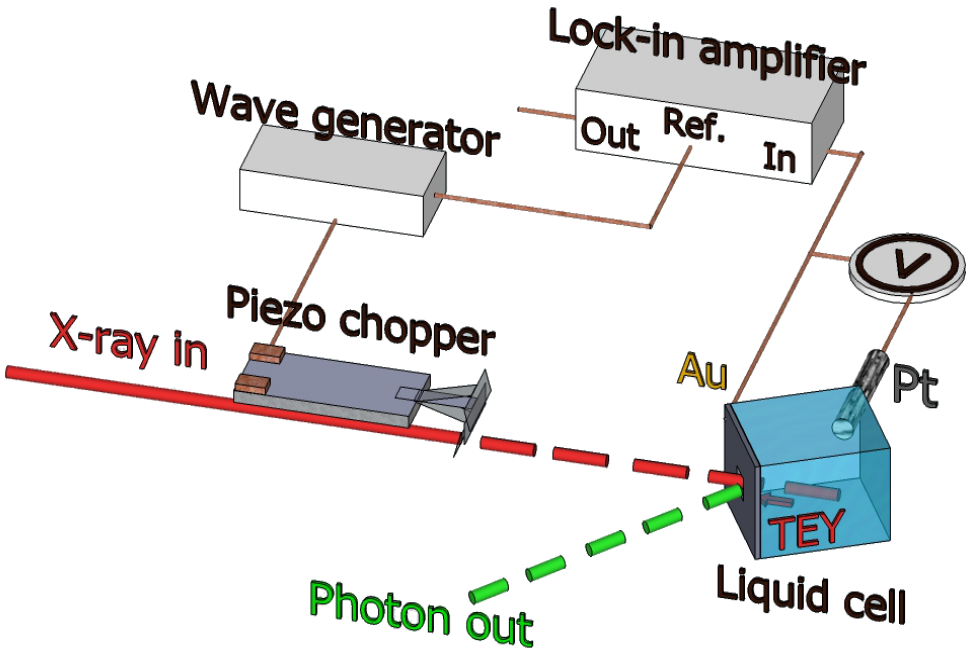

Figure S3

Schematic of the modulation set-up of the incoming x-ray beam by a piezo-actuated chopper and the TEY detection by a lock-in amplifier.

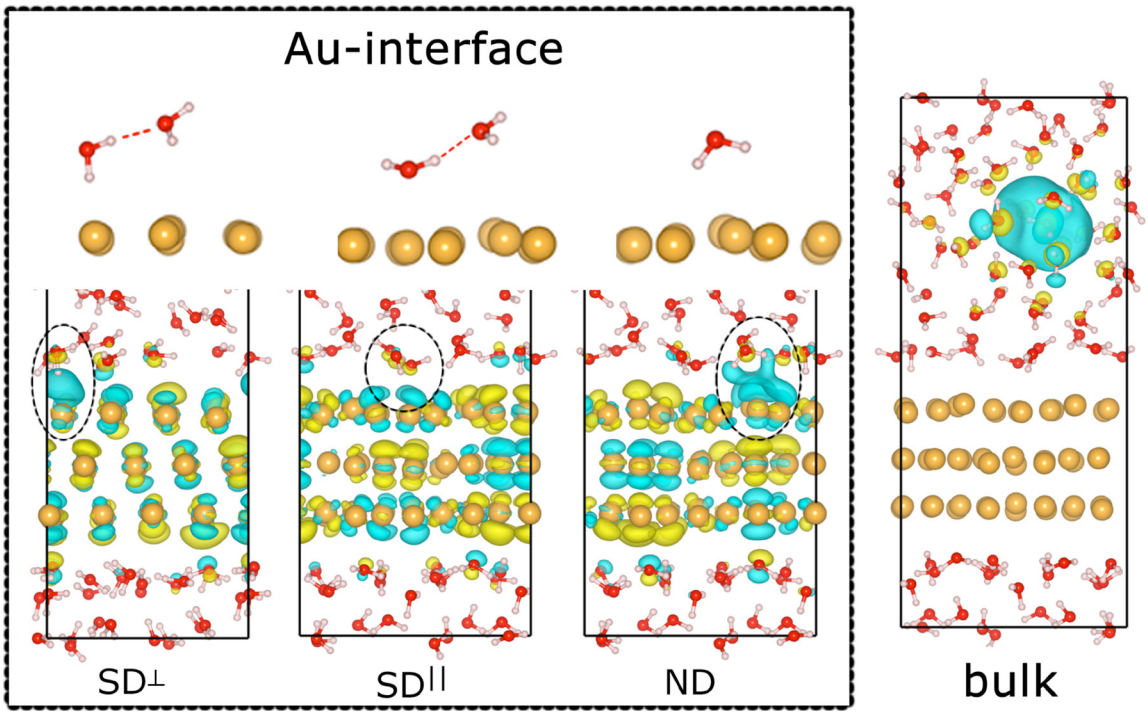

Figure S4

Representative electron densities of core-excited state resulting from the absorption of a 535 eV X-ray photon by an oxygen (red) atom. We adopt the convention that the positive phase of the density is colored blue while the negative phase is colored yellow. The hydrogen (silver) and gold (gold) atoms are shown. The excited water molecule is indicated by the dotted black ellipses. *Left box:* Electron density for water molecules in the 1st surface layer next to the gold surface. Inset: Schematic representation of SD$^{\perp}$, SD|| and ND species. The broken (black dashed line) and formed (red dashed line) donor hydrogen bonds are demonstrated. *Right:* Electron density for a core-excited SD$^{\perp}$ water molecule in the bulk (away from the interface).

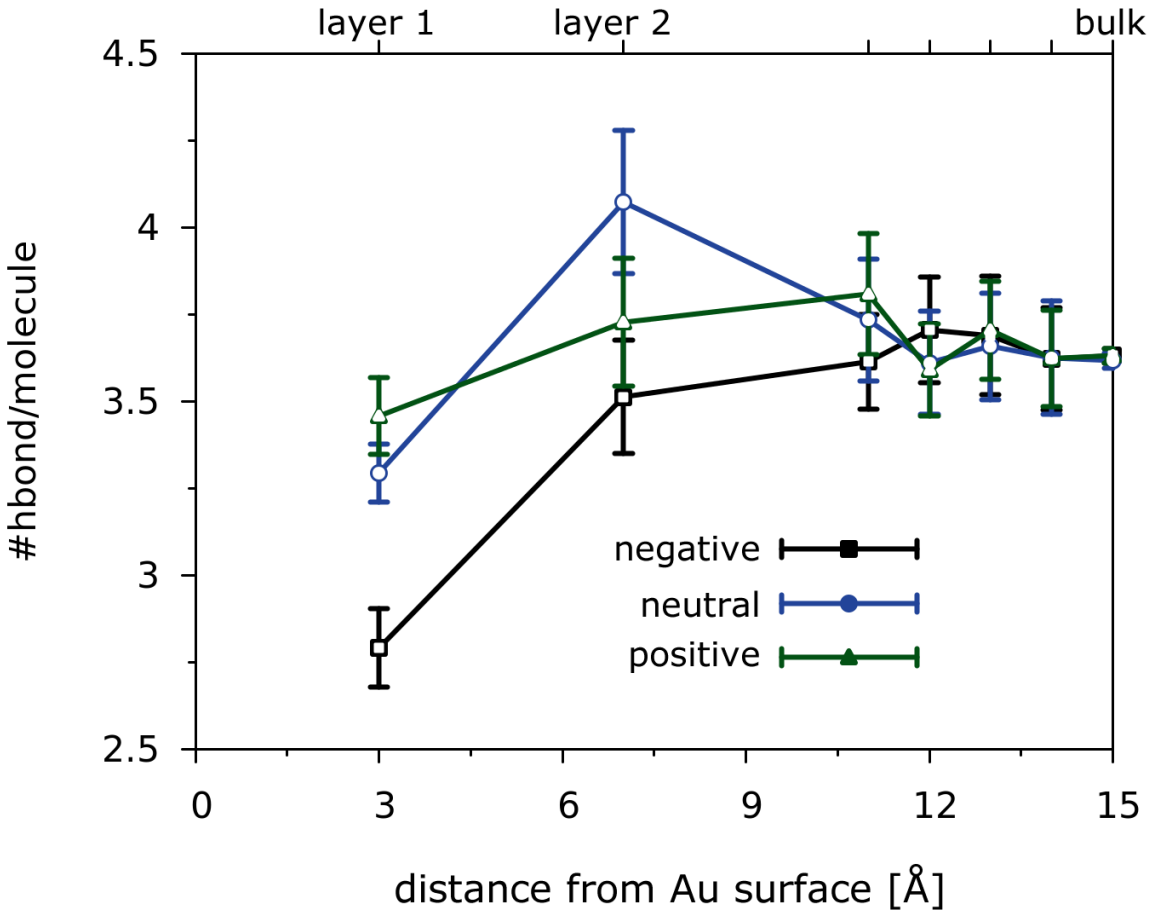

Figure S5

Hydrogen bond profile as a function of distance from the gold surface. Results for a negatively (black squares), neutral (blue circles) and positively (green triangles) charged surface are presented.

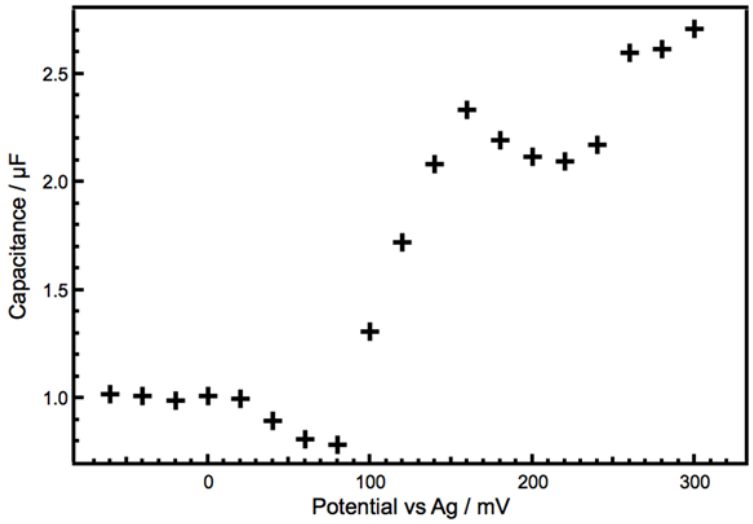

Figure S6

Capacitance measurement of the 20nm Au thin film in 10µM NaCl solution measured in the flow liquid cell. Each data point was calculated based on cyclic voltammetry curves within 20mV potential windows centered at each potential. The minimum at 80 mV corresponds to the point of zero charge.

References and Notes

1. A. J. Bard, L. R. Faulkner, *Electrochemical Methods: Fundamentals and Applications* (Wiley, New York, 1980).

2. G. Cicero, J. C. Grossman, E. Schwegler, F. Gygi, G. Galli, Water confined in nanotubes and between graphene sheets: A first principle study. *J. Am. Chem. Soc.* **130**, 1871–1878 (2008). Medline doi:10.1021/ja074418+

3. D. Chandler, Interfaces and the driving force of hydrophobic assembly. *Nature* **437**, 640–647 (2005). Medline doi:10.1038/nature04162

4. P. Fenter, L. Cheng, S. Rihs, M. Machesky, M. J. Bedzyk, N. C. Sturchio, Electrical double-layer structure at the rutile-water interface as observed in situ with small-period X-ray standing waves. *J. Colloid Interface Sci.* **225**, 154–165 (2000). Medline doi:10.1006/jcis.2000.6756

5. K. Ataka, T. Yotsuyanagi, M. Osawa, Potential-dependent reorientation of water molecules at an electrode/electrolyte interface studied by surface-enhanced infrared absorption spectroscopy. *J. Phys. Chem.* **100**, 10664–10672 (1996). doi:10.1021/jp953636z

6. M. Fleischmann, P. J. Hendra, I. R. Hill, M. E. Pemble, Enhanced Raman spectra from species formed by the coadsorption of halide ions and water molecules on silver electrodes. *J. Electroanal. Chem.* **117**, 243–255 (1981). doi:10.1016/S0022-0728(81)80086-1

7. Y. R. Shen, V. Ostroverkhov, Sum-frequency vibrational spectroscopy on water interfaces: Polar orientation of water molecules at interfaces. *Chem. Rev.* **106**, 1140–1154 (2006). Medline doi:10.1021/cr040377d

8. L. Zhang, C. Tian, G. A. Waychunas, Y. R. Shen, Structures and charging of alpha-alumina (0001)/water interfaces studied by sum-frequency vibrational spectroscopy. *J. Am. Chem. Soc.* **130**, 7686–7694 (2008). Medline doi:10.1021/ja8011116

9. V. Ostroverkhov, G. A. Waychunas, Y. R. Shen, New information on water interfacial structure revealed by phase-sensitive surface spectroscopy. *Phys. Rev. Lett.* **94**, 046102 (2005). Medline doi:10.1103/PhysRevLett.94.046102

10. J. Sung, L. Zhang, C. Tian, Y. R. Shen, G. A. Waychunas, Effect of pH on the Water/α-Al_2O_3 (1102) Interface Structure Studied by Sum-Frequency Vibrational Spectroscopy. *J. Phys. Chem. C* **115**, 13887–13893 (2011). doi:10.1021/jp2046596

11. A. Nilsson, D. Nordlund, I. Waluyo, N. Huang, H. Ogasawara, S. Kaya, U. Bergmann, L.-Å. Näslund, H. Öström, P. Wernet, K. J. Andersson, T. Schiros, L. G. M. Pettersson, X-ray absorption spectroscopy and X-ray Raman scattering of water and ice; an experimental view. *J. Electron Spectrosc. Relat. Phenom.* **177**, 99–129 (2010). doi:10.1016/j.elspec.2010.02.005

12. H. Bluhm, D. F. Ogletree, C. S. Fadley, Z. Hussain, M. Salmeron, The premelting of ice studied with photoelectron spectroscopy. *J. Phys. Condens. Matter* **14**, L227–L233 (2002). doi:10.1088/0953-8984/14/8/108

13. A. Nilsson, L. G. M. Pettersson, Chemical bonding on surfaces probed by X-ray emission spectroscopy and density functional theory. *Surf. Sci. Rep.* **55**, 49–167 (2004). doi:10.1016/j.surfrep.2004.06.002

14. J.-H. Guo, Y. Luo, A. Augustsson, J. E. Rubensson, C. Såthe, H. Agren, H. Siegbahn, J. Nordgren, X-ray emission spectroscopy of hydrogen bonding and electronic structure of liquid water. *Phys. Rev. Lett.* **89**, 137402 (2002). Medline doi:10.1103/PhysRevLett.89.137402

15. O. Fuchs, F. Maier, L. Weinhardt, M. Weigand, M. Blum, M. Zharnikov, J. Denlinger, M. Grunze, C. Heske, E. Umbach, A liquid flow cell to study the electronic structure of liquids with soft X-rays. *Nucl. Instruments Methods A* **585**, 172–177 (2008). doi:10.1016/j.nima.2007.10.029

16. T. Tokushima, Y. Horikawa, H. Arai, Y. Harada, O. Takahashi, L. G. Pettersson, A. Nilsson, S. Shin, Polarization dependent resonant x-ray emission spectroscopy of D_2O and H_2O water: Assignment of the local molecular orbital symmetry. *J. Chem. Phys.* **136**, 044517 (2012). Medline doi:10.1063/1.3678443

17. J.-H. Guo, Y. Luo, A. Augustsson, S. Kashtanov, J. E. Rubensson, D. K. Shuh, H. Agren, J. Nordgren, Molecular structure of alcohol-water mixtures. *Phys. Rev. Lett.* **91**, 157401 (2003). Medline doi:10.1103/PhysRevLett.91.157401

18. P. Jiang, J.-L. Chen, F. Borondics, P.-A. Glans, M. W. West, C.-L. Chang, M. Salmeron, J. Guo, In situ soft X-ray absorption spectroscopy investigation of electrochemical corrosion of copper in aqueous $NaHCO_3$ solution. *Electrochem. Commun.* **12**, 820–822 (2010). doi:10.1016/j.elecom.2010.03.042

19. A. Braun, K. Sivula, D. K. Bora, J. Zhu, L. Zhang, M. Grätzel, J. Guo, E. C. Constable, Direct observation of two electron holes in a hematite photoanode during photoelectrochemical water splitting. *J. Phys. Chem. C* **116**, 16870–16875 (2012). doi:10.1021/jp304254k

20. See supplementary materials in *Science* Online.

21. S. Ghosal, J. C. Hemminger, H. Bluhm, B. S. Mun, E. L. Hebenstreit, G. Ketteler, D. F. Ogletree, F. G. Requejo, M. Salmeron, Electron spectroscopy of aqueous solution interfaces reveals surface enhancement of halides. *Science* **307**, 563–566 (2005). Medline doi:10.1126/science.1106525

22. M. A. Brown, M. Faubel, B. Winter, X-Ray photo- and resonant Auger-electron spectroscopy studies of liquid water and aqueous solutions. *Annu. Rep. Prog. Chem. Sect. C* **105**, 174 (2009). doi:10.1039/b803023p

23. D. Prendergast, G. Galli, X-ray absorption spectra of water from first principles calculations. *Phys. Rev. Lett.* **96**, 215502 (2006). Medline doi:10.1103/PhysRevLett.96.215502

24. U. Bergmann, P. Wernet, P. Glatzel, M. Cavalleri, L. Pettersson, A. Nilsson, S. Cramer, X-ray Raman spectroscopy at the oxygen K edge of water and ice: Implications on local structure models. *Phys. Rev. B* **66**, 092107 (2002). doi:10.1103/PhysRevB.66.092107

25. A. H. England, A. M. Duffin, C. P. Schwartz, J. S. Uejio, D. Prendergast, R. J. Saykally, On the hydration and hydrolysis of carbon dioxide. *Chem. Phys. Lett.* **514**, 187–195 (2011). doi:10.1016/j.cplett.2011.08.063

26. W. S. Drisdell, R. Poloni, T. M. McDonald, J. R. Long, B. Smit, J. B. Neaton, D. Prendergast, J. B. Kortright, Probing adsorption interactions in metal-organic frameworks using X-ray spectroscopy. *J. Am. Chem. Soc.* **135**, 18183–18190 (2013). Medline doi:10.1021/ja408972f

27. P. Wernet, D. Nordlund, U. Bergmann, M. Cavalleri, M. Odelius, H. Ogasawara, L. A. Näslund, T. K. Hirsch, L. Ojamäe, P. Glatzel, L. G. Pettersson, A. Nilsson, The structure of the first coordination shell in liquid water. *Science* **304**, 995–999 (2004). Medline doi:10.1126/science.1096205

28. G. Cicero, A. Calzolari, S. Corni, A. Catellani, Anomalous wetting layer at the Au(111) surface. *J. Phys. Chem. Lett.* **2**, 2582–2586 (2011). doi:10.1021/jz200989n

29. R. Nadler, J. F. Sanz, Effect of dispersion correction on the Au(1 1 1)-H_2O interface: A first-principles study. *J. Chem. Phys.* **137**, 114709 (2012). Medline doi:10.1063/1.4752235

30. D. Stacchiola, J. B. Park, P. Liu, S. Ma, F. Yang, D. E. Starr, E. Muller, P. Sutter, J. Hrbek, Water nucleation on gold: Existence of a unique double bilayer. *J. Phys. Chem. C* **113**, 15102–15105 (2009). doi:10.1021/jp904875h

31. P. J. Feibelman, Partial dissociation of water on Ru(0001). *Science* **295**, 99–102 (2002). Medline doi:10.1126/science.1065483

32. A. Michaelides, A. Alavi, D. A. King, Different surface chemistries of water on Ru[0001]: From monomer adsorption to partially dissociated bilayers. *J. Am. Chem. Soc.* **125**, 2746–2755 (2003). Medline doi:10.1021/ja028855u

33. M. Tatarkhanov, D. F. Ogletree, F. Rose, T. Mitsui, E. Fomin, S. Maier, M. Rose, J. I. Cerdá, M. Salmeron, Metal- and hydrogen-bonding competition during water adsorption on Pd(111) and Ru(0001). *J. Am. Chem. Soc.* **131**, 18425–18434 (2009). Medline doi:10.1021/ja907468m

34. G. Liu, M. Salmeron, Reversible displacement of chemisorbed n-alkanethiol molecules on Au(111) surface: An atomic force microscopy study. *Langmuir* **10**, 367–370 (1994). doi:10.1021/la00014a006

35. M. F. Toney, J. N. Howard, J. Richer, G. L. Borges, J. G. Gordon, O. R. Melroy, D. G. Wiesler, D. Yee, L. B. Sorensen, Voltage-dependent ordering of water molecules at an electrode–electrolyte interface. *Nature* **368**, 444–446 (1994). doi:10.1038/368444a0

36. S. Plimpton, Fast parallel algorithms for short-range molecular-dynamics. *J. Comput. Phys.* **117**, 1–19 (1995). doi:10.1006/jcph.1995.1039

37. Y. Wu, H. L. Tepper, G. A. Voth, Flexible simple point-charge water model with improved liquid-state properties. *J. Chem. Phys.* **124**, 024503 (2006). Medline doi:10.1063/1.2136877

38. X. Zhou, R. Johnson, H. Wadley, Misfit-energy-increasing dislocations in vapor-deposited CoFe/NiFe multilayers. *Phys. Rev. B* **69**, 144113 (2004). doi:10.1103/PhysRevB.69.144113

39. P. Schravendijk, N. van der Vegt, L. Delle Site, K. Kremer, Dual-scale modeling of benzene adsorption onto Ni(111) and Au(111) surfaces in explicit water. *ChemPhysChem* **6**, 1866–1871 (2005). Medline doi:10.1002/cphc.200400591

40. R. W. Hockney, J. W. Eastwood, *Computer Simulation Using Particles* (Taylor & Francis, New York, 1989).

41. W. Shinoda, M. Shiga, M. Mikami, Rapid estimation of elastic constants by molecular dynamics simulation under constant stress. *Phys. Rev. B* **69**, 134103 (2004). doi:10.1103/PhysRevB.69.134103

42. G. J. Martyna, D. J. Tobias, M. L. Klein, Constant-pressure molecular-dynamics algorithms. *J. Chem. Phys.* **101**, 4177 (1994). doi:10.1063/1.467468

43. M. Parrinello, A. Rahman, Polymorphic transitions in single-crystals - A new molecular-dynamics method. *J. Appl. Phys.* **52**, 7182 (1981). doi:10.1063/1.328693

44. M. E. Tuckerman, J. Alejandre, R. Lopez-Rendon, A. L. Jochim, G. J. Martyna, A Liouville-operator derived. measure-preserving integrator for molecular dynamics simulations in the isothermal-isobaric ensemble. *J. Phys. Math. Gen.* **39**, 5629–5651 (2006). doi:10.1088/0305-4470/39/19/S18

45. J. Wang, R. M. Wolf, J. W. Caldwell, P. A. Kollman, D. A. Case, Development and testing of a general amber force field. *J. Comput. Chem.* **25**, 1157–1174 (2004). Medline doi:10.1002/jcc.20035

46. G. Lippert, J. Hutter, M. Parrinello, A hybrid Gaussian and plane wave density functional scheme. *Mol. Phys.* **92**, 477–488 (2010). doi:10.1080/002689797170220

47. J. VandeVondele, M. Krack, F. Mohamed, M. Parrinello, T. Chassaing, J. Hutter, QUICKSTEP: Fast and accurate density functional calculations using a mixed Gaussian and plane waves approach. *Comput. Phys. Commun.* **167**, 103–128 (2005). doi:10.1016/j.cpc.2004.12.014

48. J. VandeVondele, J. Hutter, Gaussian basis sets for accurate calculations on molecular systems in gas and condensed phases. *J. Chem. Phys.* **127**, 114105 (2007). Medline doi:10.1063/1.2770708

49. J. P. Perdew, K. Burke, M. Ernzerhof, Generalized gradient approximation made simple. *Phys. Rev. Lett.* **77**, 3865–3868 (1996). Medline doi:10.1103/PhysRevLett.77.3865

50. S. Goedecker, M. Teter, J. Hutter, Separable dual-space Gaussian pseudopotentials. *Phys. Rev. B* **54**, 1703–1710 (1996). Medline doi:10.1103/PhysRevB.54.1703

51. M. Krack, Pseudopotentials for H to Kr optimized for gradient-corrected exchange-correlation functionals. *Theor. Chem. Acc.* **114**, 145–152 (2005). doi:10.1007/s00214-005-0655-y

52. L. Genovese, T. Deutsch, S. Goedecker, Efficient and accurate three-dimensional Poisson solver for surface problems. *J. Chem. Phys.* **127**, 054704 (2007). Medline doi:10.1063/1.2754685

53. S. Grimme, J. Antony, S. Ehrlich, H. Krieg, A consistent and accurate ab initio parametrization of density functional dispersion correction (DFT-D) for the 94 elements H-Pu. *J. Chem. Phys.* **132**, 154104 (2010). Medline doi:10.1063/1.3382344

54. G. Cicero, A. Calzolari, S. Corni, A. Catellani, Anomalous wetting layer at the Au (111) surface. *J. Phys. Chem. Lett.* **2**, 2582–2586 (2011). doi:10.1021/jz200989n

55. L. S. Pedroza, A. Poissier, M.-V. Fernández-Serra, Local order of liquid water at the electrochemical interface; http://arxiv.org/abs/1403.6482 (2014).

56. A. Luzar, D. Chandler, Hydrogen-bond kinetics in liquid water. *Nature* **379**, 55–57 (1996). doi:10.1038/379055a0

57. P. E. Blöchl, Projector augmented-wave method. *Phys. Rev. B* **50**, 17953–17979 (1994). Medline doi:10.1103/PhysRevB.50.17953

58. G. Kresse, D. Joubert, From ultrasoft pseudopotentials to the projector augmented-wave method. *Phys. Rev. B* **59**, 1758–1775 (1999). doi:10.1103/PhysRevB.59.1758

59. G. Kresse, J. Furthmüller, Efficiency of ab-initio total energy calculations for metals and semiconductors using a plane-wave basis set. *Comput. Mater. Sci.* **6**, 15–50 (1996). doi:10.1016/0927-0256(96)00008-0

60. G. Kresse, J. Hafner, Ab initio molecular dynamics for liquid metals. *Phys. Rev. B* **47**, 558–561 (1993). Medline doi:10.1103/PhysRevB.47.558

61. D. Vanderbilt, Soft self-consistent pseudopotentials in a generalized eigenvalue formalism. *Phys. Rev. B* **41**, 7892–7895 (1990). Medline doi:10.1103/PhysRevB.41.7892

62. P. Giannozzi, S. Baroni, N. Bonini, M. Calandra, R. Car, C. Cavazzoni, D. Ceresoli, G. L. Chiarotti, M. Cococcioni, I. Dabo, A. Dal Corso, S. de Gironcoli, S. Fabris, G. Fratesi, R. Gebauer, U. Gerstmann, C. Gougoussis, A. Kokalj, M. Lazzeri, L. Martin-Samos, N. Marzari, F. Mauri, R. Mazzarello, S. Paolini, A. Pasquarello, L. Paulatto, C. Sbraccia, S. Scandolo, G. Sclauzero, A. P. Seitsonen, A. Smogunov, P. Umari, R. M. Wentzcovitch, QUANTUM ESPRESSO: A modular and open-source software project for quantum simulations of materials. *J. Phys. Condens. Matter* **21**, 395502 (2009). Medline doi:10.1088/0953-8984/21/39/395502

63. E. L. Shirley, Optimal basis sets for detailed Brillouin-zone integrations. *Phys. Rev. B* **54**, 16464–16469 (1996). Medline doi:10.1103/PhysRevB.54.16464

64. D. Prendergast, S. G. Louie, Bloch-state-based interpolation: An efficient generalization of the Shirley approach to interpolating electronic structure. *Phys. Rev. B* **80**, 235126 (2009). doi:10.1103/PhysRevB.80.235126

65. M. Taillefumier, D. Cabaret, A.-M. Flank, F. Mauri, X-ray absorption near-edge structure calculations with the pseudopotentials: Application to the K edge in diamond and α-quartz. *Phys. Rev. B* **66**, 195107 (2002). doi:10.1103/PhysRevB.66.195107